JGR Space Physics

RESEARCH ARTICLE
10.1029/2019JA027499

FDTD Modeling of High-Frequency Waves Through Ionospheric Plasma Irregularities

D. R. Smith[1], C. Y. Huang[2], E. Dao[2], S. Pokhrel[3], and J. J. Simpson[1]

[1]ECE Department, University of Utah, Salt Lake City, UT, USA, [2]Geospace Environment Impacts and Applications Branch, Air Force Research Laboratory, Kirtland AFB, Kirtland, NM, USA, [3]COMSOL, Inc, Los Altos, CA, USA

Key Points:
- Maxwell's equations are solved to model electromagnetic wave propagation through ionospheric plasma irregularities of polar cap patches
- Cumulative distribution function polar cap patch profiles are generated using defense meteorological satellite program data
- Transmission coefficients are calculated for various unperturbed/perturbed and unmagnetized/magnetized ionospheric conditions

Correspondence to:
D. R. Smith,
dallinsmith9@gmail.com

Citation:
Smith, D. R., Huang, C. Y., Dao, E., Pokhrel, S., & Simpson, J. J. (2020). FDTD modeling of high-frequency waves through ionospheric plasma irregularities. *Journal of Geophysical Research: Space Physics*, *125*, e2019JA027499. https://doi.org/10.1029/2019JA027499

Received 7 OCT 2019
Accepted 25 FEB 2020
Accepted article online 27 FEB 2020

Abstract Electromagnetic wave scattering and scintillation can occur at high latitudes of the Earth when polar cap patches are present. Polar cap patches range in size from 100 to 1,000 km and have densities on the order of 2–10 times that of the background ionosphere. Within polar cap patches, plasma irregularities caused by gradient drift instabilities are observed throughout the patch as elongated slivers. These irregularities vary in size from centimeters to tens of kilometers. Three major challenges must be overcome to thoroughly study high-frequency electromagnetic wave interactions with polar cap patches: (1) the complex geometrical features of the irregularities within the patches must be accommodated; (2) the non-approximated Maxwell's equations should be solved to account for all the physics of electromagnetic wave propagation, scattering, diffraction, etc.; and (3) the physics of electromagnetic wave interactions with magnetized ionospheric plasma must be included. In this paper, the finite-difference time-domain (FDTD) method is used to overcome the above three challenges and solve for electromagnetic wave interactions with plasma irregularities within a polar cap patch. Irregularities and patch profiles are generated using Defense Meteorological Satellite Program data and incorporated into the FDTD model. The transmission coefficients for high-frequency electromagnetic wave propagation through perturbed and unperturbed ionospheres, as well as for magnetized and unmagnetized ionospheric plasma ionospheres are calculated. From these simulations, the effects of small-scale irregularities on high-frequency propagation are observed.

1. Introduction

1.1. Polar Cap Patches

Polar cap patches were discovered in 1984 by Weber et al. (1984) when images from 630.0-nm all-sky imagers displayed patch-like high electron densities. Since then many scientists have extensively studied the inherent properties of polar cap patches and their effect on radio communication (see reviews by Basu et al., 1990; Crowley, 1996; Dandekar & Bullet, 1999; and Carlson, 2012).

A polar cap patch is a large quantity of plasma consisting of molecular ions and electrons. The patch-like structure has a 2–10× higher electron density concentration than the ambient electron density of the ionosphere (Weber et al., 1984). The patches follow a general two-cell convection pattern and travel with velocities of 0.5–3 km/s in the anti-sunward direction under the influence of polar cap convection. The horizontal lengths of these plasma patches range from 100 to 1,000 km. The longevity of the patch depends on their size; they can last for a couple of hours (Carlson et al., 1984; Crowley, 1996).

Many theories have been proposed to explain the existence and evolution of polar cap patches. Challenges still exist, however, due to the complex nature of the magnetosphere-ionosphere-thermosphere (MIT) coupling. This coupling drives the patch's behavior such as the F-region entry, transpolar evolution, and exit. One theory that is widely accepted is that temporal perturbations in the southward interplanetary magnetic field (IMF) cause particle precipitation through the dayside cusp of the Earth at high latitudes, thus causing polar cap patches (Carlson, 2012).

1.2. Trans-Ionospheric Signal Disturbances

Polar cap patches are often associated with radio disturbances of trans-ionospheric signals, such as those associated with Global Navigation Satellite Systems (GNSS) (Aarons, 1982). Plasma instabilities within polar cap patches cause communication impairment at high frequencies (HF: 3–30 MHz) and up into the

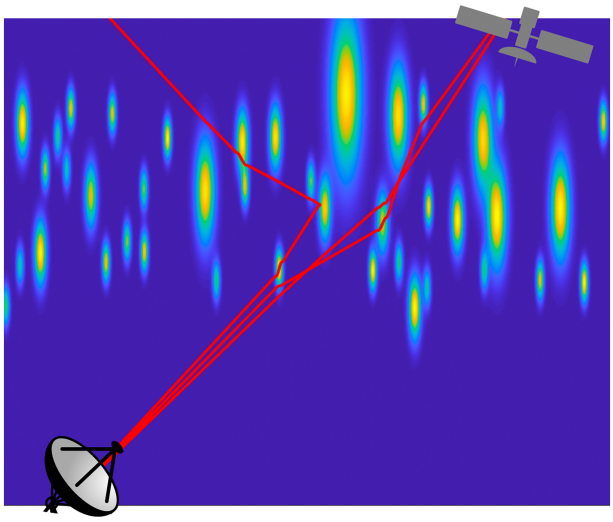

Figure 1. Schematic illustrating vertical field-align irregularities in a polar cap patch as well as example GNSS electromagnetic signals interacting with irregularities and undergoing refraction and scattering.

ultra-high frequency (UHF: 0.3–3 GHz) part of the electromagnetic spectrum. The impairment causes degradation in the form of radio scintillation, phase and time delay, trajectory misalignment, and errors in Doppler shifts (Bust & Crowley, 2007).

The irregularities are a result of the convection of the patch in the polar cap region. These plasma instabilities cause inhomogeneous magnetic field-aligned structures called irregularities. The irregularities can be characterized as elongated slivers with steep electron density gradients, and they can range in size from centimeters to tens of kilometers (Bust & Crowley, 2007). The plasma instabilities are more prevalent on the edges and trailing side of the patch (Cerisier et al., 1985; Milan et al., 2002), implying that gradient drift instability is the primary candidate for the formation of the irregularities (Basu et al., 1990).

The irregularities are aligned along the Earth's magnetic field. Thus, at high latitudes both the magnetic field and irregularities are oriented in the radial direction, as shown in Figure 1. This means that the electromagnetic signals are not normally incident on the irregularities. As a result of the disturbed conditions, most of the signal energy is directed out into space rather than to the satellite receivers due to refraction and scattering.

1.3. The Study of Signal Disturbances Caused by Irregularities

HF propagation may be used to study the structure of the irregularities in a polar cap patch. Coherent-scatter radars such as the Super Dual Auroral Radar Network (SuperDARN) observe the scattered signal components known as HF radar "echoes." HF waves are extremely sensitive to the magnetic field-aligned plasma density irregularities since the HF's wavelength is comparable in size or smaller than those of the irregularities (Chisham et al., 2007; Greenwald et al., 1995). Consequently, HF radar echoes are generated by the steep gradients (Ponomarenko et al., 2009) of the field-aligned small-scale irregularity structures (Baker et al., 1986; Moen et al., 2002). The echoes are difficult to capture due to the limited number of radar observing stations and also because of the orientation of the irregularities (see Figure 1) (Rogers et al., 2003; Warrington et al., 1997). Only the electromagnetic waves that reach the receivers of the radar station may be used as observed scattered data (Greenwald et al., 1985).

Additionally, numerical modeling may be used to study the behavior of polar cap patches as well as the propagation of electromagnetic waves through the patches. For example, the formation of polar cap patches, the transpolar evolution and convection, and the development of gradient drift instabilities in the patches have been modeled (Gondarenko & Guzdar, 1999; Sojka et al., 1993). Zaalov et al. (2003), Liu et al. (2012), Villain et al. (1984) simulated HF propagation in polar cap patches using the numerical ray tracing method to demonstrate the scattering effects of polar cap patches on radio waves. Deshpande et al. (2014) created an ionospheric scintillation model using the numerical multiple phase screen method to simulate GNSS scintillations due to irregularities (see a comprehensive review of scintillation models by Priyadarshi, 2015).

While most of modeling has been done on constructing synthetic polar cap patches or simulating radio scintillation, to the authors' knowledge no work has been done to model the transmission and scattering of HF waves within polar cap patches using a full-vector Maxwell's equations solver. Some of the difficulties of modeling the backscatter arise by the computational electromagnetic method used such as ray tracing or phase screen method which do not fully incorporate all physical phenomena that could occur from the interaction with the irregular plasma.

1.4. FDTD Modeling of Electromagnetic Propagation Through Polar Cap Patches

For the first time, the finite-difference time-domain (FDTD) method is used to simulate the propagation of electromagnetic waves through irregular plasma structures in polar cap patches. The FDTD method solves the full-vector Maxwell's equations to simulate electromagnetic wave propagation. As the name implies, the FDTD method operates in the time domain, thus allowing it to model arbitrary (realistic) source waveforms having wide frequency bandwidths. Spatially, the FDTD grid can account for complex geometrical structures (such as an inhomogeneous, perturbed ionosphere) while accounting for all of the scattering and diffraction,

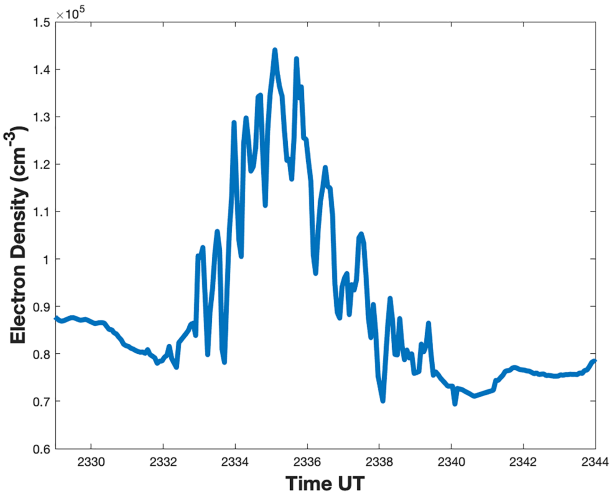

Figure 2. The electron density of the polar cap patch captured by DMSP satellite F17 on 11 December 2009.

etc., of electromagnetic wave propagation through that ionosphere (Taflove & Hagness, 2005). All of the important physics of magnetized ionosphere plasma on electromagnetic wave propagation is accounted for using FDTD update equations for Maxwell's equations coupled with the plasma momentum equation (Pokhrel et al., 2018).

The goal of this work is to demonstrate for the first time the robustness of the FDTD method in modeling scattering of HF propagation from irregularities in a polar cap patch. The FDTD method provides unique advantages over traditional modeling methods, such as ray tracing, as will be discussed in section 6. The remainder of this paper is organized as follows. In section 2, measurement data provided by the Defense Meteorological Satellite System (DMSP) are used to generate ionospheric profiles with polar cap patch irregularity structures characterized using a cumulative distribution function. Section 3 describes the FDTD grid including both the ionospheric profiles and propagating HF electromagnetic waves. Sections 4 and 5 describe the results of the simulations by producing the transmission coefficients through a perturbed and unperturbed ionosphere. Section 6 provides a discussion of the modeling motivation and results. Section 7 concludes the paper.

2. Generation of an Ionospheric Profile for a Polar Cap Patch

2.1. Irregularities in a Polar Cap Patch From DSMP Data

Generating ionospheric profiles is challenging because of the insufficient high-latitude empirical and observational electron density data, especially in 2-D/3-D for polar cap patches. However, modeling the irregularities in a polar cap patch was previously performed for other modeling purposes. Rufenach (1975), Shkarofsky (1968), and Costa and Kelley (1977) generated simple anisotropic power law irregularity spectrum plots.

A polar cap patch profile is generated using DMSP data. Specifically, the electron density profiles from the DMSP data are used to characterize the shapes, physical lengths, and plasma densities of the irregularities within the patch. Since the satellites only detect the plasma density along a line of sight, the irregularities may only be characterized along a one-dimensional (1-D) line across its physical length.

Measurement data from 11 December 2009 is used in the FDTD modeling. On that date, a polar cap patch was observed by several DMSP satellites (F15, F16, and F17). These satellites passed and detected the polar cap patch at different times and recorded its characteristics, such as the electron density as a function of time. The satellites have a sampling rate of either 1 or 4 s. Figure 2 provides an example of the DMSP electron density measurement of the polar cap patch from satellite F17. The satellite's orbit is at 840 km altitude and travels at a speed of approximately 7.5 km/s.

From Figure 2, the polar cap patch is identified along with its irregularities. The patch has steep gradients and has a higher density by a factor of two to three above the background electron density.

With sampling rates of 4 s for F15 and 1 s for F16 and F17, the smallest structures or irregularities that the satellites are able to capture range from 15 to 60 km in length. However, based on observed wave backscatter, the expected lengths of the irregularities within a physical patch extend well below 15 km and even down to cm in scale.

2.2. The Cumulative Distribution Function

The electron density irregularities observed in the DMSP data are analyzed and used to generate a histogram of the sizes of the irregularities within the polar cap patch. This is done by parsing the electron density plots of each dataset. To find the physical length of the irregularities, the local minima was found in the patch datasets. Since the data are a function of time, the data are converted into spatial dimensions using the known speed of the satellite. The data from all three satellites are consolidated together to make a single overall histogram.

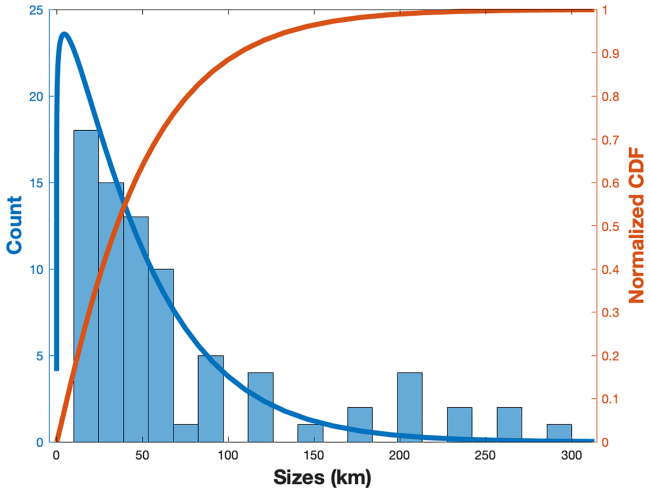

Figure 3. A histogram of the irregularity sizes from the DMSP data (blue bars). A Weibull distribution is fitted to the histogram to obtain a probability density function (left axis). The cumulative distribution function obtained from the Weibull distribution is shown (right axis).

It is well known (Little & Matheson, 1973) that the distribution of irregularities within a patch follows a power law spectrum as a function of size. The power law function describes the distribution of the irregularity sizes in a localized region. Overall, a power law function is found to fit well with the histogram generated by the DMSP satellite data from 11 December 2009. The use of a power law function is convenient; however, it is not an ideal probability density function. This is due to the fact that as the irregularities become smaller in size, the number of irregularities increases to infinity. This results in a nearly 100% probability for extremely small irregularities, yielding a noisy system instead of a practical exponential function.

Instead, the Weibull distribution is commonly used for particle size distributions because an upper limit on the number of small irregularities within a patch may be defined (Bayat et al., 2015). To capture the vast range of irregularity sizes, the fitted Weibull function is extrapolated down to 4.5 m to obtain the number of the smaller irregularities below 15 km. The fitted Weibull distribution as shown in Figure 3 as a blue line is used to characterize the irregularities in a synthetic polar cap patch profile to be used in the FDTD model.

The cumulative distribution function is obtained by taking the integral of the normalized Weibull distribution function. To accomplish this, the cumulative distribution function is discretized into sections, representing quantization for the sizes of irregularities. The difference of two points on the cumulative distribution function is calculated and provides the probability for a particular irregularity size as shown in equation (1).

$$P(a < X < b) = C_x(b) - C_x(a) \tag{1}$$

2.3. Generation of Polar Cap Patch Profiles

The cumulative distribution function describes the horizontal length distribution of irregularities that exist within a polar cap patch. Fully three-dimensional (3-D) profiles are needed, however, to populate the ionosphere in the 3-D FDTD model.

The shape of polar cap patch irregularities has been described as being elongated slivers (Bust & Crowley, 2007) that point approximately radially outward along the Earth's magnetic field near the Pole. Here, the shapes of the irregularities are approximated as prolate spheroids, where the diameter of semiaxes are determined by the cumulative distribution function. The distance from the center to the pole is randomly selected as three times the semiaxis distance (randomly selected due to lack of relevant measurements/knowledge).

The cumulative distribution function is used to populate the modeled polar cap patch using the resolution of the FDTD grid cells (4.5 m) and the size of the grid ($3.6 \times 3.6 \times 250$ km in the x, y, and z directions, respectively). A total of 25 irregularity sizes are modeled in the FDTD grid ranging from 4.5 m (corresponding to the size of one grid cell) to 1 km. The largest irregularity that is currently modeled is limited to 1 km in order to keep the required computational resources reasonable. The grid is populated starting with the largest irregularities first and then proceeding with the smaller size irregularities (see Figures 4a and 4b).

After the irregularities are determined, the plasma density is assigned to each irregularity by a Gaussian distribution. The distribution is proportional to the size of the irregularity. In general, the density of the irregularities can range from a factor of 2 to 10 times the background plasma. In this study to match the DMSP data, a low-density polar cap patch is modeled with irregularities having a range of densities that are a factor of one to three times the background.

The modeled polar cap patch is located in F region of the polar ionosphere, where the background F-region ionosphere density may be roughly approximated by a Gaussian distribution. The background electron concentration in the polar region has a density of ~9.0E4 1/cm^3 which is equivalent to a plasma frequency of ~2.7 MHz. Figure 5a shows the background ionosphere (unperturbed ionosphere). The ionosphere's F

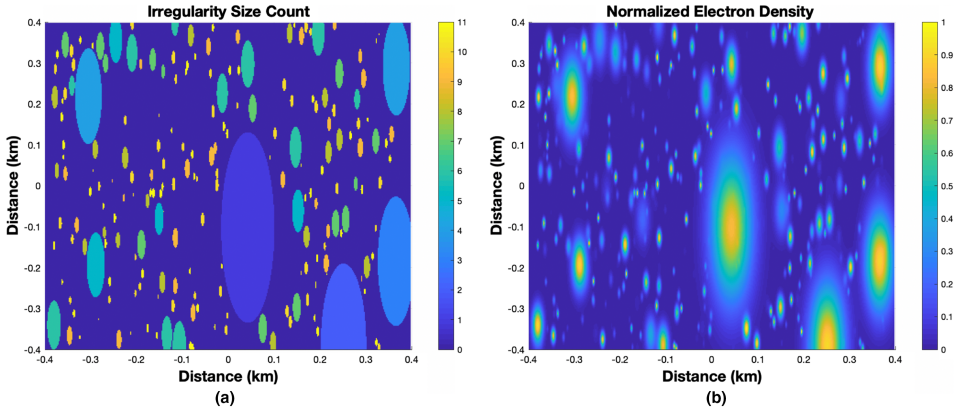

Figure 4. 2-D zoomed-in slices of the profile used in the 3-D FDTD model to represent a polar cap patch. The figure on the left (Figure 4a) shows a zoomed-in version of the irregularities being populated. The color represents the irregularity sizes. Note that the zoomed-in view and chosen color bar visualizes only 11 of the 25 sizes used in the 3-D model. The figure on the right (Figure 4b) shows the irregularities modulated with a Gaussian distribution for the electron density.

region peaks around 350 km in altitude with a standard deviation of 200 km. Along the z-axis, the FDTD grid extends from 200 to 450 km in altitude.

The irregularities in Figure 4b perturb the ionospheric background of Figure 5a by forming negative perturbations. Figure 5b shows the perturbed ionosphere representing a polar cap patch with its irregularities.

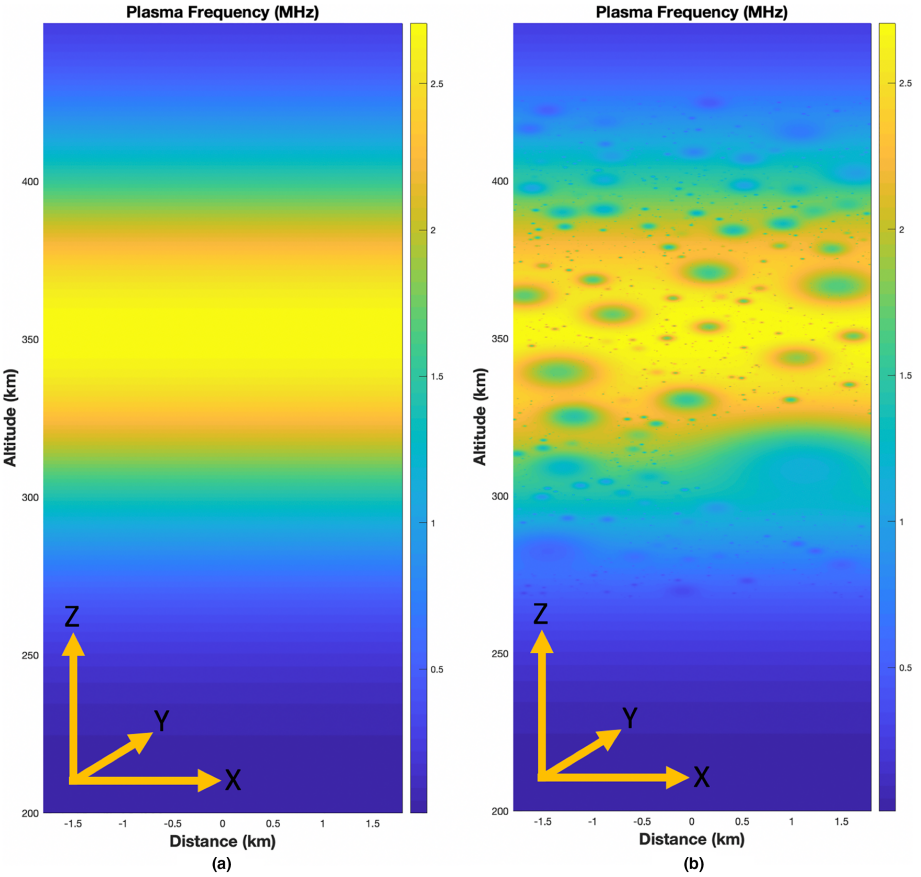

Figure 5. 2-D slice of the modeled 3-D unperturbed ionosphere profile representing the F region of the ionosphere (Figure 5a). 2-D slice of the modeled 3-D perturbed ionosphere with a polar cap patch present with its irregularities (Figure 5b). The color scheme corresponds to the plasma frequency. Note that the aspect ratio for the images are not equal, and the irregularities are highly elongated in the vertical (Z) direction.

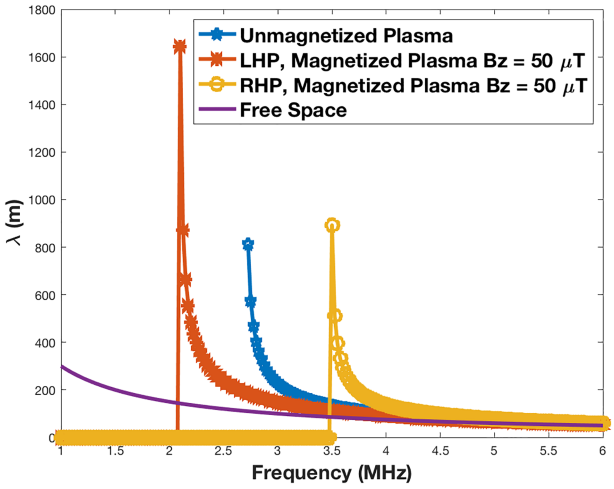

Figure 6. The dispersion relationship for the electromagnetic wavelength as a function of frequency for free space, unmagnetized plasma, and magnetized plasma (for left-hand polarization [LHP] and right-hand polarization [RHP]). The plasma frequency is set to a constant 2.7 MHz (peak frequency).

3. FDTD Model Description

The unperturbed and perturbed ionosphere profiles generated in section 2 and shown in Figure 5 are incorporated into separate 3-D FDTD grids. As mentioned earlier, the FDTD model has dimensions of $3.6 \times 3.6 \times 250$ km in the x, y, and z directions, respectively. The grid resolution is 4.5 m in all Cartesian directions (i.e., $\Delta x = \Delta y = \Delta z = 4.5$ m). The grid extends in the z direction from 200 to 450 km in the F region of the ionosphere. Starting the grid at an altitude of 200 km makes the FDTD model more computationally feasible, since the grid resolution is so high (4.5 m). The FDTD models are parallelized to run on 4400 processors of a supercomputer.

The source is a plane wave (Taflove et al., 2005) vertically incident from the bottom of the grid with an amplitude of 1 V/m. A plane wave source is used because the wave has propagated well into the far-field region of the ground antenna once it has reached an altitude of 200 km. The initial polarization of the plane wave at 200 km places the electric field along the y direction. The edges of the grid in the x and y directions of the grid are periodic boundaries since an actual polar cap patch would extend in reality much farther than the 3.6 km extent of the FDTD grid.

HF frequencies up to 6 MHz are modeled. Figure 6 shows the dispersion relation of the wavelength as a function of frequency in free space, unmagnetized ionospheric plasma, and magnetized plasma ($B_z = 50$ μT) at the peak plasma density of the ionosphere. The magnetized plasma splits the wave into left-hand polarization (LHP) and right-hand polarization (RHP) waves. The calculation shows that the 4.5 m grid resolution ensures that there are at least 10 grid cells per wavelength even at the highest frequencies.

The FDTD governing equations are coupled to equation (2) (Pokhrel et al., 2018; Samimi & Simpson, 2014), which is the plasma momentum equation. Equation (2) accounts for the electrons in the plasma ionosphere. Only electrons are modeled in the plasma because the ions are primarily motionless under the short timescales due to their large mass. In equation (2), J_e represents the plasma current density, ν_e is the collision frequency, ε is the electrical permittivity of the medium, ω_{pe} is the plasma angular frequency, and ω_B is the cyclotron frequency.

$$\frac{\partial \vec{J}_e}{\partial t} + \nu_e \vec{J}_e = \varepsilon \omega_{pe}^2 \vec{E} - \vec{\omega}_B \times \vec{J}_e \tag{2}$$

Equation (2) is initialized to zero at the beginning of the simulation (as are the electric and magnetic fields). The electron density profiles are constant in time throughout the simulation, starting at $t = 0$. The simulation ran for a total time of 150 μs. The irregularities are expected to move 2–3 km/s, so over the total simulation time of 150 μs, the irregularities would only move 0.3 m, which is smaller than the resolution of the model. For this reason, the plasma momentum equation (2) is derived assuming a constant electron density. Note that equation (2) accounts for all important ionospheric effects on the propagation of electromagnetic waves, including absorption, refraction, phase and group delay, frequency shift, polarization, and Faraday rotation.

Maxwell's equations are updated using a time step increment Δt set to 1.0 ns. This value is chosen to satisfy the Courant limit shown in equation (3) for free space (Taflove et al., 2005) as well as the magnetized plasma stability condition.

$$\Delta t < \frac{1}{c} \frac{1}{\sqrt{\frac{1}{\Delta x^2} + \frac{1}{\Delta y^2} + \frac{1}{\Delta z^2}}} \tag{3}$$

To avoid numerical dispersion, the plasma frequency and cyclotron frequency must satisfy the Nyquist sampling theorem, where the sampling frequency should be at least twice the highest frequency component (collisions at these altitudes may be neglected):

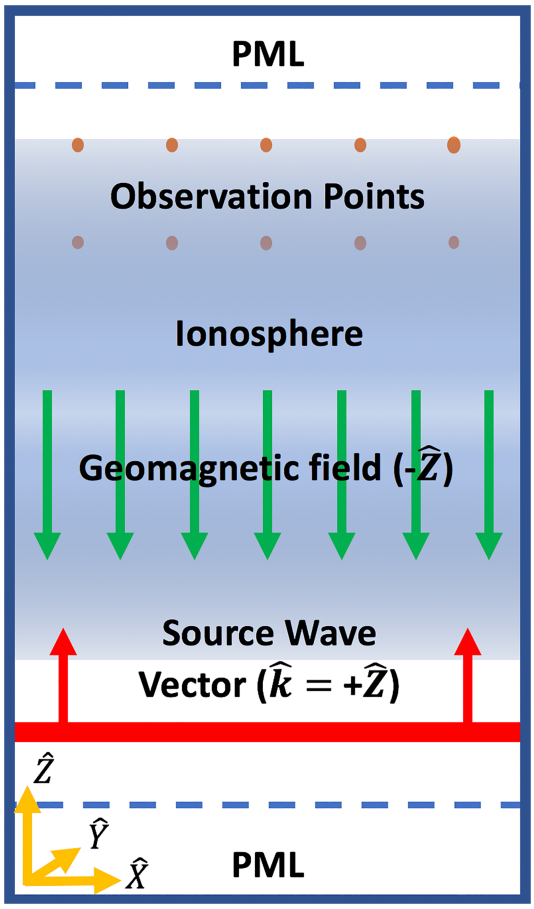

Figure 7. Diagram of the FDTD grid with PML absorbing boundary conditions on the top and bottom and periodic boundary conditions connecting the left and right sides. The source is a plane wave incident from the bottom (from the direction of the ground) in the +z direction. Observation points (orange dots) near the top capture the electric field at various locations. The geomagnetic field lines are shown as green arrows pointing in the −z direction.

$$\Delta t < \frac{1}{2\omega_B}, \tag{4a}$$

$$\Delta t < \frac{1}{2\omega_{pe}}. \tag{4b}$$

The Earth's magnetic field is set to 50 μT along the vertical (z) direction. This shows up in the cyclotron frequency as described in equation (5). The cyclotron resonance dramatically influences the propagation of the electromagnetic field when the cyclotron frequency is comparable to or greater than the plasma frequency and electromagnetic frequency of the wave.

$$\omega_B = 2\pi f = \frac{qB}{m} \tag{5}$$

The FDTD model includes perfectly matched layers (PML) on the (+z) top and (−z) bottom edges of the grid as absorbing boundary conditions to eliminate any reflections from the boundaries (Taflove et al., 2005). The PML has a thickness of 270 m to absorb all of the simulated HF wavelengths. The x and y edges do not need an absorbing boundary since they are periodic boundaries.

Two types of source time-waveforms are used. The first type is a Gaussian modulating a sinusoidal centered at 3 MHz and having a bandwidth of 3 MHz. This type of source is used to investigate the power transmission through the ionosphere. The second type of source is a sinusoidal signal. This source type is used to capture 2-D images of the electromagnetic scattering in the ionosphere.

Observation points are included in the FDTD grid to study the reflection and transmission through the F region of the ionosphere. The observation points are placed above the ionosphere before the PML boundary. The observation points record the E_x and E_y components at every time step. A diagram of the FDTD grid is presented in Figure 7.

Two types of FDTD models are run: (1) one including the profiles generated in section 2 and (2) a free space model. The observation points in the free space model are used when calculating the transmission coefficients (as the incident wave). Several cases of the Type 1 simulations are run: (1) an unperturbed ionosphere (without a polar cap patch) with no magnetic field, (2) an unperturbed ionosphere with a 50 μT magnetic field in the z direction, and (3) a perturbed ionosphere (with a polar cap patch) using the same magnetic field conditions.

4. Results for an Unperturbed Ionosphere

Observation points capture the electric field components above the ionosphere (at 445 km in altitude) in order to calculate the transmission coefficients. With a critical plasma frequency peak of 2.7 MHz of the ionosphere, complete reflection is expected below 2.7 MHz in the unperturbed ionosphere.

The discrete Fourier transform is performed on the recorded electric field components to determine the magnitude of the signal in the frequency domain. This same process is done for the electric fields recorded in the free space grid. The transmission coefficients are found by taking the ratio of the magnitude in the ionospheric profile models (E_I) and the free space model (E_F) as shown using equation (6).

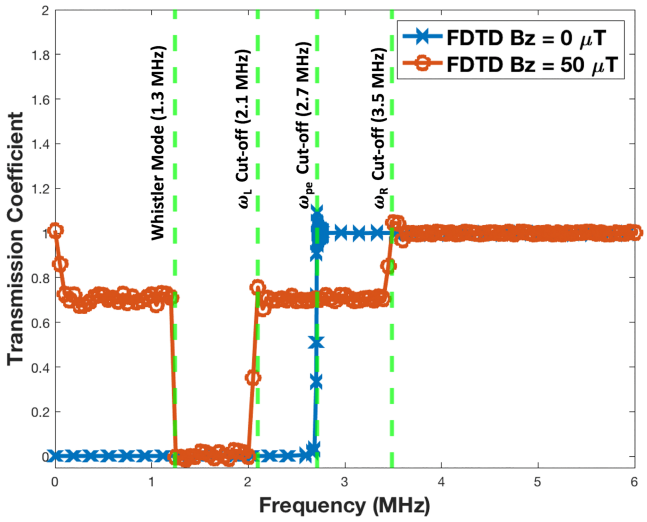

Figure 8. The transmission coefficients as a function of frequency for unperturbed ionospheres. Results are shown for an unmagnetized plasma (blue line) and a magnetized plasma with 50 μT vertical magnetic field (red line). The green dash lines are the cutoff frequencies for each mode.

$$\Gamma = \frac{E_I}{E_F} \tag{6}$$

Figure 8 plots the transmission coefficients incident on an unperturbed ionosphere profiles (Figure 5a) without a background magnetic field (blue line) and including a vertical magnetic field of 50 μT (red line). Analytical results calculated by the dispersion relationships (Fridman & Kennedy, 2004) in equation (7a) for unmagnetized plasma condition and equation (7b) for magnetized plasma are superimposed on the FDTD-calculated results in Figure 8.

$$1 - \frac{\omega_{pe}^2}{\omega^2} = 0 \tag{7a}$$

$$1 - \frac{\omega_{pe}^2}{\omega^2}\left(\frac{1}{1 \pm {}^{\omega_B}/_{\omega}}\right) = 0. \tag{7b}$$

As shown in Figure 8, the propagating frequencies above the critical frequency of the ionosphere (2.7 MHz) are transmitted at 100% for the unmagnetized case ($B_z = 0$ μT). Right at the critical frequency the abrupt discontinuity causes an oscillatory behavior known as Gibbs phenomenon (Proakis & Manolakis, 2007) due to the sampling rate in the FDTD model. For the case of a magnetized plasma, the FDTD-calculated results show that the magnetic field splits the critical frequency for the RHP and LHP waves. The cutoff frequencies for each mode are presented as green dash lines. The magnetized plasma case shows the low-frequency whistler mode.

5. Results for a Perturbed Ionosphere

The polar cap patch profile (Figure 5b) is incorporated into the FDTD model and analogous simulations as discussed in section 4 are performed. Figure 9 plots the transmission coefficients for the perturbed ionosphere profile for the case of a 50 μT background magnetic field and also without a magnetic field. The red and blue lines are obtained from two example observation points, whereas the yellow and purple lines are the average (mean) values from all of the observation points combined (625 in total).

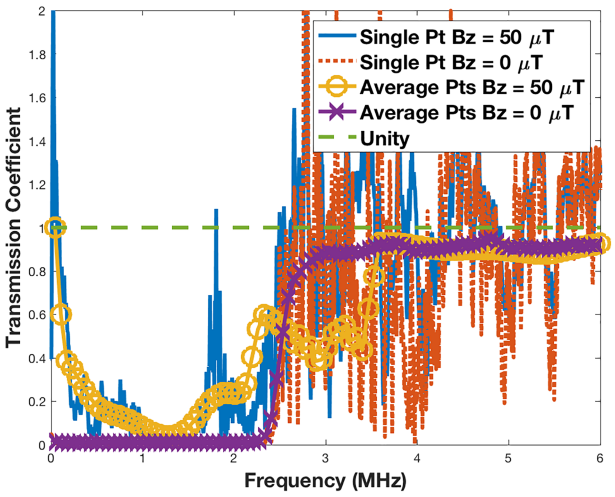

Figure 9. The plot shows the transmission coefficients as a function of frequency for a perturbed ionosphere. Results from two individual example observation points are shown as well as the mean value (average) from all of the observation points combined. A green dashed line is added to show where 100% of the wave is transmitted.

In Figure 9, the purple and yellow (average) results have similar characteristics (cutoff frequency behavior) as for the unperturbed ionosphere of Figure 8. The noise appearing in the blue and red (single point) results shows that the polar cap patch is interacting with the electromagnetic waves in a complex manner, allowing energy to transmit or scatter throughout the polar cap patch above the critical frequency (2.7 MHz) of the ionosphere. The transmission coefficients of the blue and red line extend above unity. This is due to constructive interference that is occurring from all of the scattered waves at the observation point.

In Figure 9, the transmission coefficient for the averaged results at 6 MHz is nearly 90%, compared to 100% for the unperturbed ionosphere as shown in Figure 8. The power loss indicates that 10% of the wave is scattered back toward the ground as HF backscatter or echoes. This backscatter occurs for a vertically upward propagation direction from the source that is parallel to both the geomagnetic field and elongation direction of the plasma instabilities. This angle of incidence (high elevation angle) of the source may occur at high latitudes. Also observed in Figure 9 relative to Figure 8 is that the range of frequencies that are transmitted is shifted, allowing lower frequencies to transmit.

Screenshots of the electromagnetic waves were captured in Figures 10a and 10b. Specifically, Figures 10a and 10b show a zoomed-in view of the

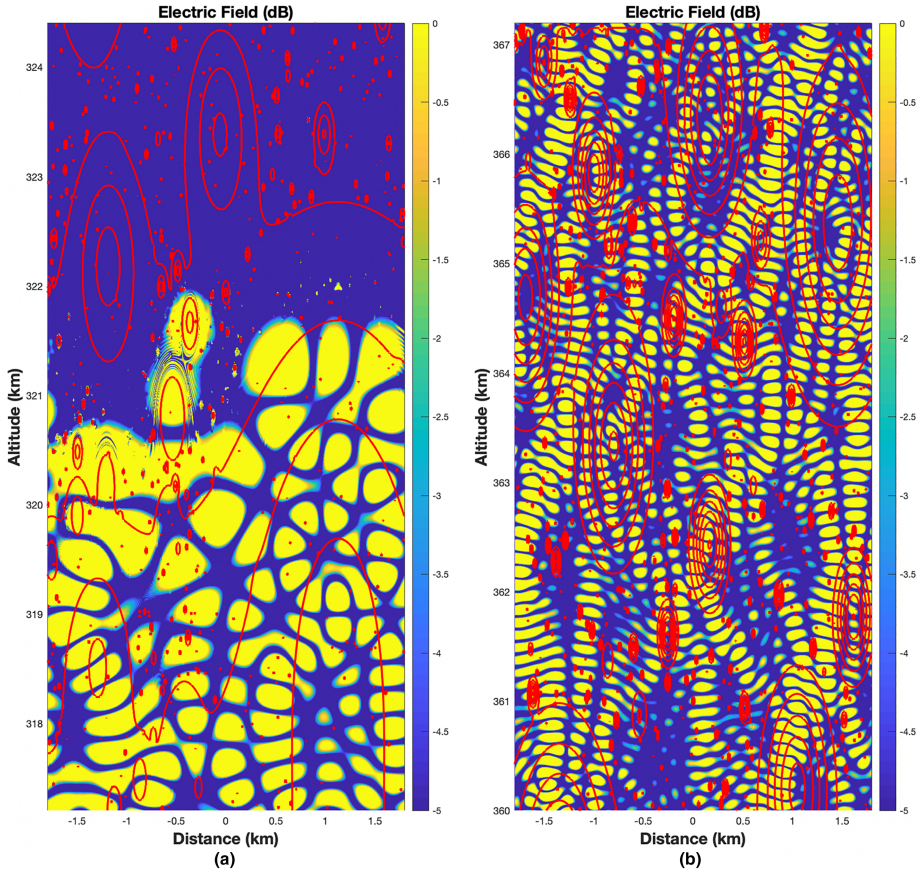

Figure 10. A zoomed-in view of the electromagnetic wave propagation in a perturbed ionospheric profile. The red lines are contours of the irregularities and background ionosphere. Figure 10b is at 2 MHz and Figure 10b is at 4 MHz. The 2 MHz signal is reflected but still interacts with the larger irregularities. Figure 10b shows additional scattering as the higher frequency 4 MHz wave encounters the irregularities and is transmitted. Note that the images are at different locations of the model.

FDTD-calculated wave propagation at two example frequencies and across a range of altitudes at a snapshot in time. The figures show the power of the electric field overlaid with the ionospheric profile as red contour lines in red. Figure 10a shows results for 2 MHz and at the altitude where total reflection is occurring. Figure 10b shows results for a 4 MHz signal interacting with the irregularities.

6. Discussion

Radar networks, such as SuperDARN and EISCAT, utilize HF propagation to study the magnetosphere-ionosphere-thermosphere environment at high and low latitudes of the Earth. One primary area of study is plasma entry and convection across the polar region. To study this phenomenon, HF electromagnetic waves are directed toward irregularity structures in polar cap patches. The ionospheric irregularities cause the sensitive HF waves to refract, diffract, disperse, and scatter. Some of the scattering returns back to Earth and may be detected. The backscatter may include useful information, i.e., unique group delays, Doppler frequency shifts, phase delays, and echo amplitudes, which are used to characterize the plasma in the ionosphere.

If there is a basic understanding of how HF electromagnetic waves interact with ionospheric irregularities, then any measured backscattered HF signals may be studied and used to characterize ionospheric irregularities. This knowledge may then be used to better understand plasma convection from radar network data.

The irregularities in the F-region magnetized ionospheric plasma are anisotropic and elongated along the magnetic field lines. The scattering is dependent on the characteristics of the irregularities and orientation of the propagation. Therefore, the ionospheric irregularity parameters that affect electromagnetic

scattering are electron intensity, spatial distribution, orientation, structural size, and shape (polar-to-equatorial radius ratio) with respect to the incident wave propagation (Ponomarenko et al., 2009). Maximum scattering occurs when the spatial spectrum of the electron density fluctuation (width of the irregularity) along the propagation direction is double the propagation wavelength (Booker, 1956). Thus, satisfying the Bragg scatter condition.

The ray tracing method has been the primarily tool to simulate backscattering from ionospheric irregularities. However, the ray tracing method is limited for this application because it is an optical geometric solver. That is, several assumptions and simplifications are made to describe the physical interaction of electromagnetic wave propagation with plasma irregularities, since it cannot account for wave theory.

For example, one simplification made in ray tracing is that the backscattering may only occur when the electromagnetic propagation is sufficiently refracted such that the wave vector is orthogonal to the vertical magnetic field. This is known as the orthogonality condition. The orthogonality condition has been assumed since 1970 (Bates & Albee, 1970) and is utilized in every ray tracing model for studying backscattering from plasma irregularities. At high latitudes the orthogonality condition implies that there would be little backscatter for high elevation angles.

Although more computationally demanding, the FDTD method has many advantages over ray tracing. First, it does not assume the orthogonality condition. Second, FDTD can model electromagnetic interactions with irregularities on a subwavelength level, whereas ray tracing cannot model small irregularity structures that are comparable in size to the wavelength of the HF waves. This is because ray tracing is a geometrical solver and assumes that objects are much larger than the wavelength.

According to the authors' knowledge, the work described herein represents the first time the FDTD method has been applied to HF propagation though plasma irregularities in polar cap patches. The modeling and results are unique in that the full-vector Maxwell's equations are solved and also the resolution of the model is extremely fine (4.5 m) compared to the wavelength of the HF waves. With such high resolution, the FDTD model simultaneously modeled a wide distribution of irregularities from 1 km down to 4.5 m. From this work, the interaction of ionospheric irregularities on electromagnetic waves were investigated on a subwavelength level.

The FDTD model simulated a range of frequencies for various scenarios such as unmagnetized/magnetized and unperturbed/perturbed ionospheric environments. The transmission coefficient was calculated from each scenario to measure a general overall interaction of the ionospheric profiles. Figure 9 showed that there is backscatter for high elevation angles (in our case, vertically upward propagation) when the orthogonal condition is not satisfied. In the case of Figure 9, 10% of the total energy was scattered back for transmitted frequencies above the plasma frequency.

The FDTD model used equation (2), the plasma momentum equation, to model the cold magnetized plasma using electron densities from DMSP data. The plasma momentum equation assumed a constant electron density since the model simulated a duration of only 150 μs, which is too short for the electron density to evolve in any impactful way. Furthermore, the collision frequency is neglected and is approximated to zero, since collisions would have little effect on the HF wave propagation in the F region of the ionosphere (Zawdie et al., 2017).

Source frequencies from 1 to 6 MHz were simulated in the model. It would be advantageous to model higher frequencies; however, higher frequencies were not considered here in order to keep the computational demands of the model more reasonable. FDTD requires at least 10 grid cells per wavelength to avoid numerical dispersion, so higher frequencies would require higher grid resolutions and thus larger models, computer memory, and simulation times. As a result, the FDTD model may be applied to higher frequencies and applications such as SuperDARN by simply increasing the grid spatial resolution to maintain at least 10 grid cells per wavelength and by correspondingly increasing the time step increment.

7. Conclusions and Future Work

Irregularities in polar cap patches impair trans-ionospheric HF radio signals by causing refraction, scattering, and power loss. Computational electrodynamics modeling of HF propagation through polar cap patches can provide unique insights into this electromagnetic propagation phenomenon that is difficult to measure

in real life. In particular, 3-D FDTD modeling is advantageous for this application. The grid-based FDTD method can account for the complex geometries and compositions of the irregularity structures in a straightforward manner. In this paper, irregularities ranging from 4.5 m to 1 km were modeled and were seen to impact vertical HF propagation by causing refracting, scattering, and diffraction. The FDTD results were found to compare well with analytical results. Also, the average transmission coefficient for a perturbed ionosphere was found to have similar characteristics (cutoff frequency behavior) as for the transmission coefficient for an unperturbed ionosphere. One major difference, however, was a 10% energy loss in the transmission due to scattering from the irregularities despite the incident angle not satisfying the orthogonality condition.

Future work will include a sensitivity study to investigate the impact on HF backscatter of the orientation of the geomagnetic field (which will impact the elongation direction of the irregularities), and the irregularity size, shape, magnitude, and spatial densities. The FDTD method will be able to provide backscatter information such as unique group delays, Doppler frequency shifts, phase delays, and echo amplitudes. The results may be compared with Booker's (1956) work on scattering from irregularities for verification.

An investigation will also be conducted into traditional electromagnetic solvers used in this field, primarily the ray tracing method, to verify or improve as needed the assumptions and conditions used to model backscatter. For example, the orthogonality condition will be further tested and compared with physical data. This future work may highlight additional advantages of the FDTD method compared to the ray tracing method for this application.

Acknowledgments
This project was supported by an Internship with the Air Force Research Laboratory (AFRL) Space Scholar Program and by the Air Force Office of Scientific Research under Grants LRIR 18 RVCOR127. All data is available Smith, Dallin (2020): Data for Paper 1. figshare. Dataset. https://doi.org/10.6084/m9.figshare.11632926.v1. The support and resources from the Center for High Performance Computing at the University of Utah are gratefully acknowledged.

References

Aarons, J. (1982). Global morphology of ionospheric scintillation. *Proceedings of the IEEE*, *70*(4), 360–378. https://doi.org/10.1109/PROC.1982.12314

Baker, K. B., Greenwald, R. A., Walker, A. D. M., Bythrow, P. F., Zanetti, L. J., Potemra, T. A., et al. (1986). A case study of plasma processes in the dayside cleft. *Journal of Geophysical Research*, *91*(A3), 3130. https://doi.org/10.1029/JA091iA03p03130

Basu, S., Basu, S., MacKenzie, E., Coley, W. R., Sharber, J. R., & Hoegy, W. R. (1990). Plasma structuring by the gradient drift instability at high latitudes and comparison with velocity shear driven processes. *Journal of Geophysical Research*, *95*(A6), 7799–7818. https://doi.org/10.1029/JA095iA06p07799

Bates, H. G., & Albee, P. R. (1970). Aspect sensitivity of F layer HF backscatter echoes. *Journal of Geophysical Research*, *75*, 165–170. https://doi.org/10.1029/JA075i001p00165

Bayat, B., Rastgo, M., Zadeh, M. M., & Vereecken, H. (2015). Particle size distribution models, their characteristics and fitting capability. *Journal of Hydrology*, *529*, 872–889. https://doi.org/10.1016/j.jhydrol.2015.08.067

Booker, H. G. (1956). A theory of scattering by nonisotropic irregularities with application for radar reflections from aurora. *Journal of Atmospheric and Terrestrial Physics*, *8*, 2004–2221.

Bust, G. S., & Crowley, G. (2007). Tracking of polar cap ionospheric patches using data assimilation. *Journal of Geophysical Research*, *112*, A05307. https://doi.org/10.1029/2005JA011597

Carlson, H. C. (2012). Sharpening our thinking about polar cap ionospheric patch morphology, research, and mitigation techniques. *Radio Science*, *47*, RS0L21. https://doi.org/10.1029/2011RS004946

Carlson, H. C. Jr., Wickwar, V. B., Weber, E. J., Buchau, J., Moore, J. G., & Whiting, W. (1984). Plasma characteristics of polar cap F layer arcs. *Geophysical Research Letters*, *11*, 895–898.

Cerisier, J. C., Berthelier, J. J., & Beghin, C. (1985). Unstable density gradients in the high-latitude ionosphere. *Radio Science*, *20*(4), 755–761. https://doi.org/10.1029/RS020i004p00755

Chisham, G., et al. (2007). A decade of the Super Dual Auroral Radar Network (SuperDARN): Scientific achievements, new techniques and future directions. *Surveys in Geophysics*, *28*(1), 33–109. https://doi.org/10.1007/s10712-007-9017-8

Crowley, G. (1996). Critical review on ionospheric patches and blobs. In W. R. Stone (Ed.), *The Review of Radio Science 1992-1996* (Vol. 1, pp. 619–648). New York: Oxford University Press.

Dandekar, B. S., & Bullet, T. W. (1999). Morphology of polar cap patch activity. *Radio Science*, *24*, 1187–1205.

Deshpande, K. B., Bust, G. S., Clauer, C. R., Rino, C. L., & Carrano, C. S. (2014). Satellite-beacon ionospheric-scintillation Global Model of the upper Atmosphere (SIGMA) I: High-latitude sensitivity study of the model parameters. *Journal of Geophysical Research: Space Physics*, *119*, 4026–4043. https://doi.org/10.10002/2013JA0119699

Fridman, A., & Kennedy, L. A. (2004). *Plasma physics and engineering* (1st ed.). New York, NY: Taylor and Francis, Inc.

Gondarenko, N. A., & Guzdar, P. N. (1999). Gradient drift instability in high latitude plasma patches: Ion inertial effects. *Geophysical Research Letters*, *26*, 3345–3348.

Greenwald, R. A., Baker, K. B., Hutchins, R. A., & Hanuise, C. (1985). An HF phased-array radar for studying small-scale structure in the high-latitude ionosphere. *Radio Science*, *20*(1), 63–79. https://doi.org/10.1029/RS020i001p00063

Greenwald, R. A., et al. (1995). DARN/SuperDARN A global view of the dynamics of high-latitude convection. *Space Science Reviews*, *71*(1–4), 761–796. https://doi.org/10.1007/BF00751350

Little, L. T., & Matheson, D. N. (1973). Radio scintillations due to plasma irregularities with power law spectra: The interstellar medium. *Monthly Notices of the Royal Astronomical Society*, *162*, 329–338.

Liu, E. X., Hu, H. Q., Liu, R. Y., Wu, Z. S., & Lester, M. (2012). An adjusted location model for SuperDARN backscatter echoes. *Annales de Geophysique*, *30*(12), 1769–1779. https://doi.org/10.5194/angeo-30-1769-2012

Milan, S. E., Lester, M., & Yeoman, T. K. (2002). HF radar polar patch formation revisited: Summer and winter variations in dayside plasma structing. *Annales de Geophysique*, *20*, 487–499.

Moen, J., Walker, I. K., Kersley, L., & Milan, S. E. (2002). On the generation of cusp HF backscatter irregularities. *Journal of Geophysical Research*, *107*(A4), 1044. https://doi.org/10.1029/2001JA000111

Pokhrel, S., Shankar, V., & Simpson, J. J. (2018). 3-D FDTD modeling of electromagnetic wave propagation in magnetized plasma requiring singular updates to the current density equation. *IEEE Transactions on Antennas and Propagation*, *66*, 4772–4781.

Ponomarenko, P. V., St-Maurice, J.-P., Waters, C. L., Gillies, R. G., & Koustov, A. V. (2009). Refractive index effects on the scatter volumes location and Doppler velocity estimates of ionospheric HF backscatter echoes. *Annales de Geophysique*, *27*, 4207–4219.

Priyadarshi, S. (2015). A review of ionospheric scintillation models. *Surveys in Geophysics*, *36*(2), 295–324. https://doi.org/10.1007/s10712-015-9319-1

Proakis, J., & Manolakis, D. (2007). *Digital signal processing: Principles, algorithms, and applications*. London, UK: Pearson Education, Inc.

Rogers, N. C., Warrington, E. M., & Jones, T. B. (2003). Oblique ionogram features associated with off-great-circle HF propagation at high and sub-auroral latitudes. *IEEE Proc. Microwaves Antennas Propag.*, *150*(4), 295–300. https://doi.org/10.1049/ip-map:20030552

Rufenach, C. L. (1975). Ionospheric scintillation by a random phase screen: Spectral approach. *Radio Science*, *10*, 155–165. https://doi.org/10.1029/RS010i002p00155

Samimi, A., & Simpson, J. J. (2014). An efficient 3-D FDTD model of electromagnetic wave propagation in magnetized plasma. *IEEE Transactions on Antennas and Propagation*, *63*, 269–279.

Shkarofsky, I. P. (1968). Generalized turbulence space-correlation and wave-number spectrum-function pairs. *Canadian Journal of Physics*, *46*, 2133–2153. https://doi.org/10.1139/p68-562

Sojka, J. J., Bowline, M. D., Schunk, R. W., Decker, D. T., Valladares, C. E., Sheehan, R., et al. (1993). Modeling polar cap F-region patches using time varying convection. *Geophysical Research Letters*, *20*(17), 1783–1786. https://doi.org/10.1029/93GL01347

Taflove, A., & Hagness, S. C. (2005). *Computational electrodynamics: The finite-difference time-domain method*. Norwood, MA: Artech House.

Villain, J. P., Greenwald, R. A., & Vickrey, J. F. (1984). HF ray tracing at high latitudes using measured meridional electron density distributions. *Radio Science*, *19*(1), 359–374. https://doi.org/10.1029/RS019i001p00359

Warrington, E. M., Rogers, N. C., & Jones, T. B. (1997). Large HF bearing errors for propagation paths contained within the polar cap. *IEEE Proc. Microwaves Antennas Propag.*, *144*, 241–249.

Weber, E. J., Buchau, J., Moore, J. G., Sharber, R., Livingston, R. C., Winningham, J. D., & Reinisch, B. W. (1984). F layer ionization patches in the polar cap. *Journal of Geophysical Research*, *89*, 1683–1694.

Zaalov, N. Y., Warrington, E. M., & Stocker, A. J. (2003). Simulation of off-great circle HF propagation effects due to the presence of patches and arcs of enhanced electron density within the polar cap ionosphere. *Radio Science*, *38*(3), 1052. https://doi.org/10.1029/2002RS002798

Zawdie, K. A., Drob, D. P., Siskind, D. E., & Coker, C. (2017). Calculating the absorption of HF radio waves in the ionosphere. *Radio Science*, *52*, 767–783. https://doi.org/10.1002/2017RS006256